Biochimica et Biophysica Acta 1808 (2011) 1161–1169

Contents lists available at ScienceDirect

Biochimica et Biophysica Acta

journal homepage: www.elsevier.com/locate/bbamem

The amyloidogenic SEVI precursor, PAP248-286, is highly unfolded in solution despite an underlying helical tendency

Jeffrey R. Brender [a,b], Ravi Prakash Reddy Nanga [a,b], Nataliya Popovych [a,b], Ronald Soong [a,b], Peter M. Macdonald [c], Ayyalusamy Ramamoorthy [a,b,*]

[a] Department of Chemistry, University of Michigan, Ann Arbor, MI 48109-1055, USA
[b] Department of Biophysics, University of Michigan, Ann Arbor, MI 48109-1055, USA
[c] Department of Chemical and Physical Sciences, University of Toronto at Mississauga, Mississauga, Canada

ARTICLE INFO

Article history:
Received 2 December 2010
Received in revised form 12 January 2011
Accepted 18 January 2011
Available online 22 January 2011

Keywords:
Amyloid
SEVI
Natively disordered
Structure
NMR

ABSTRACT

Amyloid fibers in human semen known as SEVI (semen-derived enhancer of viral infection) dramatically increase the infectivity of HIV and other enveloped viruses, which appears to be linked to the promotion of bridging interactions and the neutralization of electrostatic repulsion between the host and the viral cell membranes. The SEVI precursor $PAP_{248-286}$ is mostly disordered when bound to detergent micelles, in contrast to the highly α-helical structures found for most amyloid proteins. To determine the origin of this difference, the structures of $PAP_{248-286}$ were solved in aqueous solution and with 30% and 50% trifluoroethanol. In solution, pulsed field gradient (PFG)-NMR and ^{1}H-^{1}H NOESY experiments indicate that $PAP_{248-286}$ is unfolded to an unusual degree for an amyloidogenic peptide but adopts significantly helical structures in TFE solutions. The clear differences between the structures of $PAP_{248-286}$ in TFE and SDS indicate electrostatic interactions play a large role in the folding of the peptide, consistent with the slight degree of penetration of $PAP_{248-286}$ into the hydrophobic core of the micelle. This is another noticeable difference between $PAP_{248-286}$ and other amyloid peptides, which generally show penetration into at least the headgroup region of the bilayer, and may explain some of the unusual properties of SEVI.

1. Introduction

Viral attachment to the surface of the target cell is the first and almost always the most difficult step in the virus life cycle [1]. The short-half life of almost all viruses in solution (~6 h for HIV) ensures that a productive infection can only be achieved if a significant number of viral particles adhere to the cell surface in a relatively narrow time window upon exposure [2]. The vast majority of viruses lack the opportunity to initiate infection due to the low occurrence of successful virus–cell encounters and the short time window available for infection; it has been estimated for the HIV virus that only approximately 1 in 100 to 1 in 1000 replication competent virions are able to establish infection in cell-free culture [3]. Because of the low efficiency of the viral adhesion process, cofactors that increase the efficiency of viral adhesion to target cells can drastically increase this ratio by allowing the virus to gain a successful beachhead before the invasion of the cell.

The ubiquity of semen in the sexual transmission of the HIV virus makes it a natural place to look for such cofactors. One such cofactor is $PAP_{248-286}$ (PAP: prostatic acid phosphatase, sequence GIHKQKEKSRLQGGVLVNEILNHMKRATQIPSYKKLIMY), a peptide fragment of prostatic acid phosphatase, a protein abundant in human semen [4]. Incubation with $PAP_{248-286}$ dramatically reduces the viral load necessary to establish a persistent infection, lowering the threshold needed from several million virions to less than 10 [4]. The exact mechanism by which $PAP_{248-286}$ enhances the infectivity of the HIV virus is unknown but is believed to enhance viral adhesion to host cell prior to receptor-specific binding by reducing the electrostatic repulsion between the membranes of the virus and the target cell [5,6]. It is noteworthy that similar degrees of enhancement have been detected in the unrelated XMRV virus as well as multiple strains of HIV, indicating the effect is likely not dependent on a particular receptor [7,8].

$PAP_{248-286}$ is inactive in the monomeric state and must first aggregate to form the active SEVI (semen enhancer of viral infection) form to promote viral infection [4,6,9]. While many species of aggregated $PAP_{248-286}$ appears to be active, $PAP_{248-286}$ is most active in the form of large aggregates with the characteristic β-sheet conformation of amyloid proteins [4,10]. Since the cross β-sheet structural motif is common to all amyloid proteins but the ability of amyloid fibers from other proteins to enhance viral infection is minor in comparison to SEVI fibers from $PAP_{248-286}$, a structural understanding of SEVI and its precursors at the atomic level is necessary to understand its mechanism of action [4,11].

* Corresponding author. Tel.: +1 734 647 6572; fax: +1 734 764 3323.
E-mail address: ramamoor@umich.edu (A. Ramamoorthy).

0005-2736/$ – see front matter © 2011 Elsevier B.V. All rights reserved.
doi:10.1016/j.bbamem.2011.01.010

Towards this end, we previously solved the high-resolution 3D structure of the SEVI precursor peptide $PAP_{248-286}$ in a membrane mimicking environment (sodium dodecyl sulfate (SDS) micelles) using NMR spectroscopy in an attempt to understand the mechanism by which SEVI promotes the bridging of viral and host cell membranes [12]. The structure of $PAP_{248-286}$ was found to be unusually disordered compared to the micelle-bound structures of other amyloidogenic proteins that are also natively unfolded in solution like SEVI [13–18]. This finding is significant because highly disordered proteins have increased interaction volumes relative to more ordered, compact proteins and are particularly efficient at promoting multiple weak interactions between binding partners such as those necessary to promote reversible membrane binding and association with endocytic nucleation factors [19–21]. If the unusual amount of conformational flexibility present in the monomeric membrane-bound $PAP_{248-286}$ is also retained in the larger SEVI aggregates [21], it may explain to some degree the unique ability of SEVI to enhance infection of enveloped viruses.

In an attempt to determine if the disordered state of the SDS bound monomer is an intrinsic property of the $PAP_{248-286}$ peptide or is a consequence of specific interactions with the SDS micelle, we have solved the structures of $PAP_{248-286}$ both in solution and in 30% and 50% trifluoroethanol, a solvent that promotes helix formation by a different mechanism than SDS and lipid bilayers. Our results show that $PAP_{248-286}$ is disordered to a greater extent than most other amyloid proteins in solution, which typically have some degree of transient structure which restricts the degrees of freedom in the native state and assists in aligning aggregation prone regions [22]. We also found that, in contrast to the disordered structure present in solution and in SDS micelles, $PAP_{248-286}$ folds into a well-ordered amphipathic helix in TFE (trifluoroethanol) solutions. This finding suggests that the disordered conformation found in SDS micelles is the result of the strong electrostatic binding of $PAP_{248-286}$ to the surface of the micelle and the superficial penetration of $PAP_{248-286}$ into the interior and is not an intrinsic property of the peptide sequence.

2. Materials and methods

2.1. Pulsed field gradient NMR spectroscopy

$PAP_{248-286}$ obtained from Biomatik (Toronto, Ontario, purity 95%) was first disaggregated using a TFA (trifluoroacetic acid)/HFIP (hexafluoroisopropanol) mixture and lyophilized as described in [12]. For each sample, 0.489 mg of disaggregated $PAP_{248-286}$ was dissolved in 500 μL of 50 mM potassium phosphate buffer with 100 mM NaCl prepared from 90% D_20/10% H_20 at either pH 7.4 or pH 6.1 to make a final concentration of 219 μM peptide. ^{1}H NMR diffusion measurements were carried out at 499.78 MHz using the stimulated echo (STE) pulsed field gradient (PFG) pulse sequence with squared gradient pulses of constant duration (5 ms) and a variable gradient amplitude along the longitudinal axis [23]. Typically, 32 transients were recorded for each spectra. To assay possible time-dependent aggregation behavior, the PFG-NMR experiment was repeated on each sample every 2 h for a total of 12 h. Typical acquisition parameters used in NMR experiments were as follows: a 90° pulse width of 23 μs, a spin echo delay of 10 ms, a stimulated echo delay of 150 ms, a recycle delay of 5 s, a spectral width of 10 kHz and 4048 data points. A saturation pulse centered at the water frequency was used for solvent suppression. Radio frequency pulses were phase cycled to remove unwanted echoes. All spectra were processed with an exponential multiplication equivalent to a 5 Hz line broadening prior to Fourier transformation and were referenced relative to tetramethylsilane (TMS). The gradient strength was calibrated ($G = 3.28\ \mathrm{T\ m^{-1}}$) from the known diffusion coefficient of HDO in D_2O at 25 °C ($D_0 = 1.9 \times 10^{-9}\ \mathrm{m^2\ s^{-1}}$) [24].

2.2. 2D NMR data collection and processing

NMR samples containing TFE were prepared from lyophilized $PAP_{248-286}$ as described in [12] and dissolved to a concentration of 1.2 mM in 20 mM phosphate buffer at pH 7.5 containing 10% D_2O and either 30 or 50% d_2-trifluoroethanol (TFE). The NMR sample for $PAP_{248-286}$ in aqueous solution was prepared similarly except the pH was 6. For each sample, 2D ^{1}H-^{1}H TOCSY (total correlation spectroscopy) and 2D ^{1}H-^{1}H NOESY (nuclear Overhauser enhancement spectroscopy) spectra were recorded in the phase sensitive mode by quadrature detection at 25 °C (TFE samples) or 37 °C (solution sample) using a 900 MHz Bruker (Billerica, MA) Avance NMR spectrometer equipped with a triple-resonance *z*-gradient cryogenic probe optimized for ^{1}H-detection. CD spectra were taken to confirm the absence of a conformational change in solution over the temperature range 25–45 °C (see Fig. S1 in Supplementary information). The TOCSY spectra were acquired using 512 t1 points, a 80 ms mixing time, and 16 scans while the NOESY spectra were acquired using 512 t1 points, a 300 ms mixing time, and 32 scans. A recycle delay of 1.5 s was used for both experiments. The WATERGATE pulse sequence was used for suppression of the water signal [25]. All spectra were zero-filled in both dimensions to yield matrices of 2048×2048 points. Proton chemical shifts were referenced to the water proton signal at 4.7 ppm. The backbone and side-chain resonances of the peptide were assigned from the TOCSY and NOESY spectra using a standard approach described elsewhere [26]. All 2D spectra were processed using NMRPIPE and TopSpin softwares and analyzed using SPARKY [27,28].

2.3. Structure calculation

NOE cross-peaks were integrated within SPARKY and converted into upper distance bounds using the CALIBA routine within CYANA. The final list included 412 total NOE restraints for the 30% TFE sample (178 intra-residual, 132 sequential, 99 medium range and 3 long range NOEs) and 550 NOE restraints for the 50% TFE sample (199 intra-residual, 175 sequential, 171 medium range and 5 long range NOEs) (see Table 1). The dihedral angle restraints used in the CYANA structure calculation were directly calculated from the medium range NOE constraints [29]. These restraints were then used to generate an ensemble of 100 low-energy conformers for each sample using the standard simulated annealing in torsion space protocol. During the first round of structure calculation, only the unambiguous long-range NOE constraints were used to generate a low-resolution fold for the structure. Assignments of the remaining ambiguous NOE cross-peaks were made in an iterative fashion by applying a structure-aided filtering strategy in further rounds of structure calculations [30]. Eight

Table 1
Statistical information for the $PAP_{248-286}$ structural ensemble in TFE.

	30% TFE	50% TFE
Distance constraints		
Total	412	550
Intra-residual	178	199
Inter-residual	234	351
Sequential ($i-j=1$)	132	175
Medium ($i-j=2, 3, 4$)	99	171
Long ($i-j\geq 5$)	3	5
Structural statistics		
Violated distance constraints	0	1
Violated angle constraints	0	0
RMSD of all backbone atoms (Å)		
Gln259–Thr275	0.49 ± 0.17	0.31 ± 0.12
RMSD of all heavy atoms (Å)		
Gln259–Thr275	1.32 ± 0.27	1.02 ± 0.25
Ramachandran plot		
Residues in most favored region (%)	74.4	86.8
Residues in additional allowed region (%)	24.1	13.2
Residues in generously allowed region (%)	1.5	0

thousand annealing steps in total were used for each sample. From these 100 conformers, the 10 lowest energy conformers were selected and visualized using MOLMOL [31].

3. Results

3.1. $PAP_{248-286}$ is significantly unfolded and exclusively monomeric when freshly dissolved in solution

Most amyloidogenic peptides that are commonly considered to be unstructured are actually in conformational equilibrium with a more ordered state that is frequently an important intermediate along the aggregation pathway, although the exact type of metastable secondary structure varies from peptide to peptide and is dependent on other factors such as the temperature and the peptide sequence. NMR spectra of amyloidogenic peptides in the monomeric state have several features in common that support the formation of transient structure in solution. First, the chemical shift and *J*-coupling values of amyloid peptides considered to be natively unfolded in solution typically deviate from the chemical shift values expected from random coil conformations [32–36]. The degree to which the chemical shifts deviate from the expected random coil values also frequently correlates with the amyloidogenicity of the sequence, suggesting that the formation of a metastable structure can drive amyloid fiber formation [32,36–38]. This finding is reinforced by ^{15}N relaxation measurements indicating regions of reduced mobility in natively unfolded amyloidogenic peptides consistent with the formation of secondary structure [40,41]. The frequent observation of strong sequential (i, $i+1$) but not medium (i, $i+3$ or $i+4$) or long-range NOEs (i, $i+\geq 5$) indicate secondary structure in these regions is likely to be transient rather than stable [32,39].

By contrast, the 2D ^1H-^1H NOESY spectra of monomeric $PAP_{248-286}$ at pH 6 has a significant spectral overlap due to poor chemical shift dispersion (Fig. 1). Although individual residues show positive chemical shift deviations consistent with the formation of transient β-sheet formation (Fig. 2), the effect is not consistent across consecutive residues and is therefore very likely to reflect differences in the electrostatic environment of the nuclei, rather than the formation of nascent secondary structure. The weak NOE cross-peak intensities apparent in the spectrum also indicate a significant degree of mobility in the structure, consistent with poorly defined or absent secondary structure.

Pulsed field gradient (PFG) NMR was employed to further probe the nature of the monomeric peptide in solution. A magnetic field gradient applied in PFG-NMR attenuates the signal of larger and hence more slowly diffusing molecules less than that of smaller and faster diffusing ones, allowing quantitative measurement of the hydrodynamic radius of the molecule from a plot of the signal intensity versus the applied gradient strength. Fig. 3 shows the 1D ^1H spectra of $PAP_{248-286}$ in the absence of a magnetic field gradient. In Fig. 4, the decay in intensity is plotted as a function of the gradient strength for $PAP_{248-286}$ at pH 7.4 after incubation for 2 and 12 h, and for pH 6.1 after 2 h. The very high degree of linearity in all the samples indicates that all the $PAP_{248-286}$ solutions are monodisperse on the millisecond timescale and not undergoing a conformational exchange which has been observed for $A\beta_{1-40}$ [42]. Further evidence for the monodispersity of the sample can be seen from the intensity decay of individual resonances. All peaks in the spectra of $PAP_{248-286}$ were found to decay at the same rate. A characteristic broad resonance near 0 ppm arising from slowly diffusing oligomers found in the PFG-NMR spectrum of IAPP and $A\beta_{1-40}$ is conspicuously absent in the $PAP_{248-286}$ sample [42,43]. The relatively high signal intensity apparent in the spectrum also suggests that, in contrast to the amyloidogenic IAPP and $A\beta_{1-40}$ peptides [42,43], the majority of the $PAP_{248-286}$ molecules are tumbling rapidly and the signal is not significantly broadened by conformational exchange. No changes in the aggregation state are observable after 12 h of incubation at 37 °C, as shown by the very high degree of similarity between the 2 and 12 h traces in Fig. 4A.

The hydrodynamic radius of $PAP_{248-286}$ measured by PFG-NMR is 1.6 nm at 37 °C at both pH 7.4 and 6.1. This value is consistent with the peptide being in the monomeric state, although a compact small

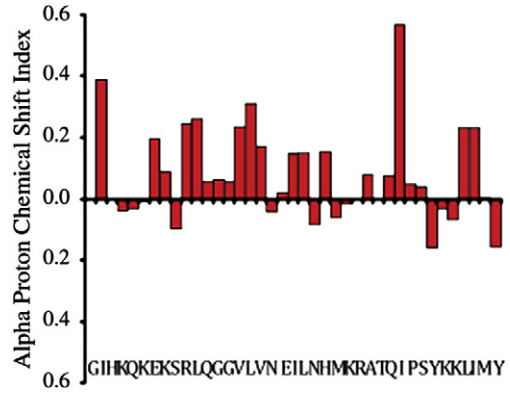

Fig. 2. Alpha proton chemical shift index (CSI) plot for $PAP_{248-286}$ in aqueous solution (50 mM KPi, pH 6). CSI values were calculated by subtracting residue-specific mean chemical shifts for the random coil state from experimental chemical shifts. Continuous stretches of residues (3 or more) with a CSI either ≤ -0.1 or ≥ 0.1 indicate a propensity for secondary structure formation. Except for a small continuous stretch of residues (V262-V264) with a positive CSI indices indicating possible nascent β-sheet formation, the CSI values are consistent with a disordered peptide.

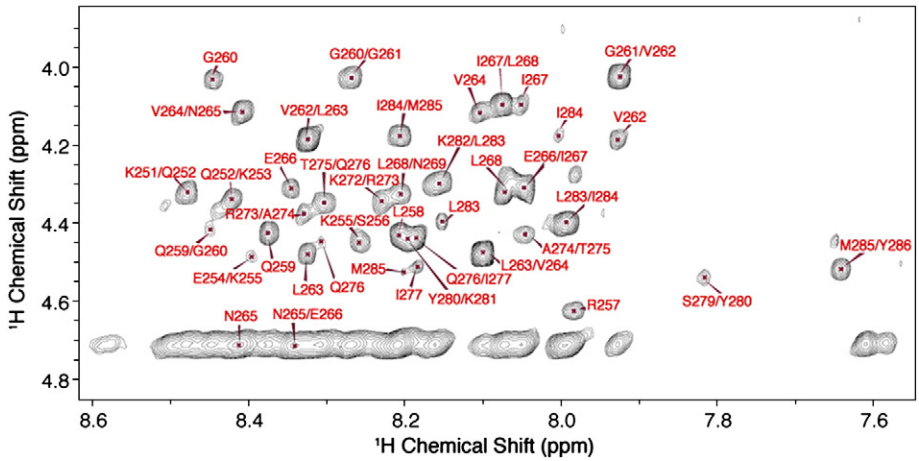

Fig. 1. The finger print region of 2D ^1H-^1H NOESY spectra of $PAP_{248-286}$ in aqueous solution (50 mM KPi, pH 6, 42 °C) showing NOE connectivities among H_α nuclei. The lack of dispersion of peaks in this region indicates $PAP_{248-286}$ is disordered in solution.

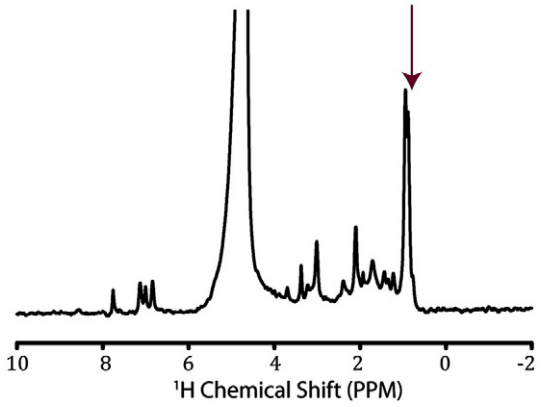

Fig. 3. ^{1}H NMR of 215 μM $PAP_{248-286}$ at 37 °C in 50 mM sodium phosphate buffer, 100 mM NaCl. The red arrow indicates the peak used for further analysis. Differences in the diffusion constant calculated from other peaks were negligible (data not shown).

oligomeric state cannot be ruled out on the basis of the hydrodynamic radius alone. However, other pieces of evidence argue for the peptide being exclusively in the monomeric state. In particular, the complete lack of secondary structure in the peptide and the lack of any change in the aggregation state over time argue against peptide self-association. The hydrodynamic radius of $PAP_{248-286}$ is similar to that reported for the non-amyloidogenic rat variant of the 37 residue IAPP peptide (1.4 nm) and highly denatured peptides of similar size (~1.8 nm) but larger than the amyloidogenic human version of the IAPP peptide (0.81 nm) and $A\beta_{1-40}$ [42–44]. The value is therefore

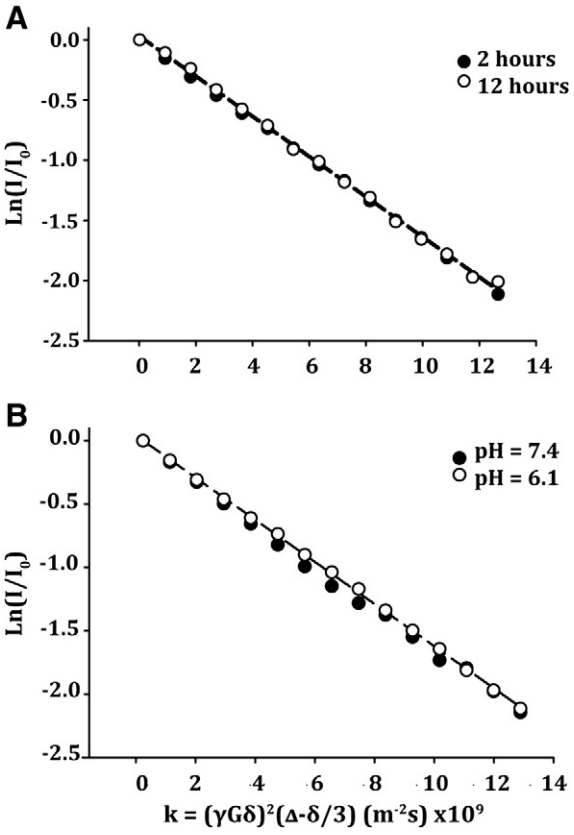

Fig. 4. (A) Normalized stimulated-echo intensity decays from STE (stimulated-echo) PFG ^{1}H NMR spectra 215 μM $PAP_{248-286}$ at 37 ° C in 50 mM sodium phosphate buffer, 100 mM NaCl pH 7.4 obtained after 2 h incubation and 12 h incubation. The slope corresponds to a hydrodynamic radius of 16 nm for both species. (B) The corresponding decays for $PAP_{248-286}$ in 50 mM sodium phosphate buffer at pH 7.4 and pH 6.1.

consistent with a significantly unfolded monomeric $PAP_{248-286}$ peptide, with a larger relative hydrodynamic radius of many other natively unfolded amyloidogenic peptides and proteins.

3.2. $PAP_{248-286}$ adopts helical structure in trifluoroethanol/water mixtures

The structure of $PAP_{248-286}$ in SDS micelles is also largely disordered, although substantially more NOE connectivities exist and the chemical shift index indicates regions of stable or metastable secondary structure (V262-H270 and Y280-I284) [12]. The lack of structure in the SDS bound form is unusual as most unfolded peptides (as opposed to proteins) adopt a helical secondary structure when bound to SDS. Several reasons may explain the lack of helical structure in the membrane-bound form of $PAP_{248-286}$. One possibility is that helical states of $PAP_{248-286}$ are intrinsically disfavored, and $PAP_{248-286}$ is therefore unable to adopt them under any circumstances. Another possibility is that while $PAP_{248-286}$ can adopt helical structures, it does not do so due to the environment of the SDS micelle. To test this possibility, we obtained 2D ^{1}H-^{1}H NOESY and 2D ^{1}H-^{1}H TOCSY and NMR spectra of $PAP_{248-286}$ in trifluorethanol/water mixtures that are known to promote the formation of α-helices in peptides.

Unlike the poorly dispersed spectra that is apparent when $PAP_{248-286}$ is dissolved in buffer, the 2D ^{1}H-^{1}H NOESY spectra of $PAP_{248-286}$ in 30% and 50% TFE solution display numerous, well-resolved cross-peaks, with a significant degree of spectral dispersion in the amide proton region. The degree of spectral dispersion is an indication of at least a partial degree of secondary structure throughout the peptide (Fig. 5), in contrast to the largely unstructured SDS bound conformer. Inter-residual $d_{\alpha HNH(i,\ i+3)}$, $d_{\alpha HNH(i,\ i+4)}$, and $d_{\alpha H\beta H(i,\ i+3)}$ NOE connectivities along with negative chemical shift indices provide further evidence for helical structure in the central region of the peptide (Figs. 6 and 7). In 30% TFE the central helical region extends from Q259-A274 with remainder of the peptide at the C- and N-terminal ends in a largely disordered conformation (Fig. 8), as shown by the absence of $d_{\alpha HNH(i,\ i+3)}$, $d_{\alpha HNH(i,\ i+4)}$ NOE connectivities at the ends of the molecule and the lack of a consistent positive or negative trend in the chemical shift values when compared to random coil values. At a higher concentration of TFE, the helical propensities of $PAP_{248-286}$ are more pronounced. In 50% TFE, the central helical region is extended at the C-terminal end, encompassing Q259-I284, with a pronounced kink caused by P278. In addition, the N-terminal end shows signs of helix formation, as indicated by the K251-L256 $d_{\alpha HNH(i,\ i+3)}$ NOE connectivities and negative chemical shift index values in this region.

4. Discussion

4.1. Structured intermediates are typically found in the misfolding pathway of amyloid proteins

Amyloid fibers are difficult to form from a completely disordered state due to the low probability that multiple aggregation prone segments will align in the correct orientation required for the precise self-assembly of the very ordered amyloid fiber [22,45]. Because it is unlikely that a totally unfolded protein will find the proper contacts to nucleate the formation of the amyloid fiber, some degree of residual structure in the monomeric protein is essential for amyloid fiber formation in natively unfolded proteins and peptides [46]. Specifically, it has been proposed by Uversky et al. that natively unfolded amyloid proteins conform to the pre-molten globule state, a denatured state that is characterized by some degree of compactness and residual structure but less than the molten globule state, from which it is separated by an all-or-none phase transition [47]. A conformational transition to a structured intermediate has therefore

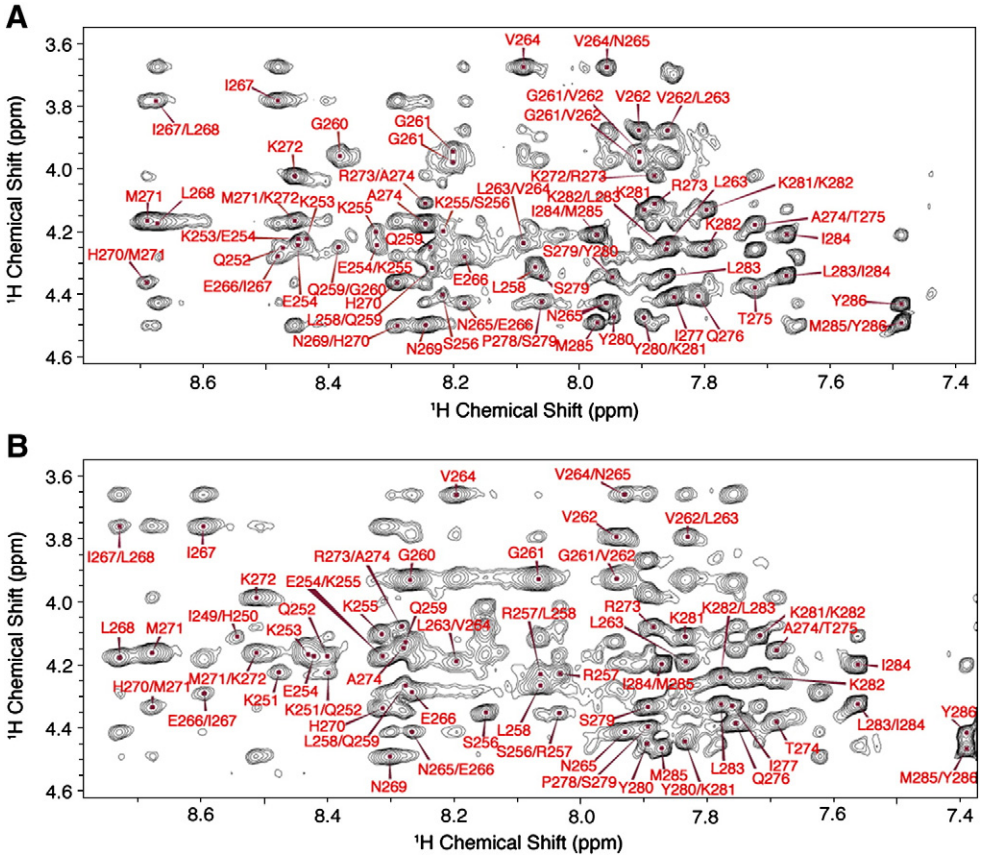

Fig. 5. The finger print region of 2D ^{1}H-^{1}H NOESY spectra of $PAP_{248-286}$ in (A) 30% TFE and (B) 50% TFE showing NOE connectivities among H_{α} nuclei. The dispersion of peaks in this region in both spectra indicates $PAP_{248-286}$ is relatively well folded in both media.

been proposed to be a critical step in the amyloidogenesis pathway for many natively unfolded proteins [46,48].

Structured intermediates have been directly observed for a number of natively unfolded amyloid peptides and proteins [49,50]. It is important to note that it is not essential that such an intermediate have the β-sheet conformation of the final amyloid product, merely that stable or metastable contacts are formed in the intermediate state that are unlikely to occur in a completely unfolded protein. In fact, helical structures in particular are common amyloidogenic intermediates [48]. This finding is of particular interest as helical structures are apparent when natively unfolded amyloid proteins bind to membranes, which are known to be strong inducers of amyloid formation for many proteins [51].

4.2. NMR results reveal that monomeric $PAP_{248-286}$ is unusually unfolded in solution

The PFG-NMR results indicate that $PAP_{248-286}$ is significantly, but not completely, unfolded in the monomeric state in solution. More specifically, the degree of compaction of the monomer is less than that of other amyloidogenic proteins of similar size that are considered to be natively unfolded but more than that of completely unfolded

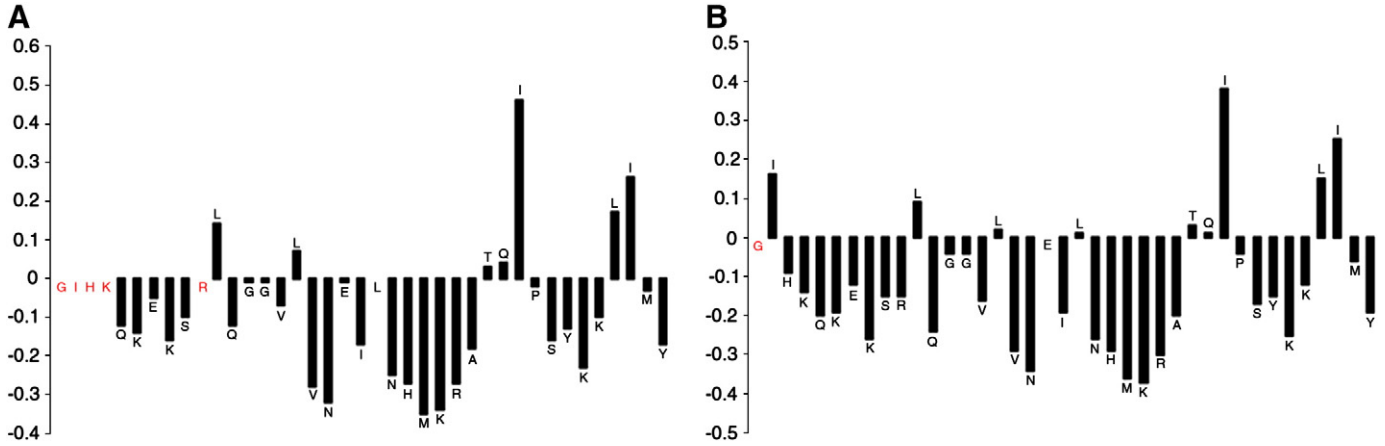

Fig. 6. Alpha proton chemical shift index (CSI) plot for $PAP_{248-286}$ in 30% TFE (gray) and 50% TFE (black). CSI values were calculated by subtracting residue-specific mean chemical shifts for the random coil state from experimental chemical shifts. Continuous stretches of residues (~3 or more) with a CSI ≤ −0.1 indicate a propensity for an α-helical conformation. The CSI for residues in red were not determined due to poor resolution for these residues.

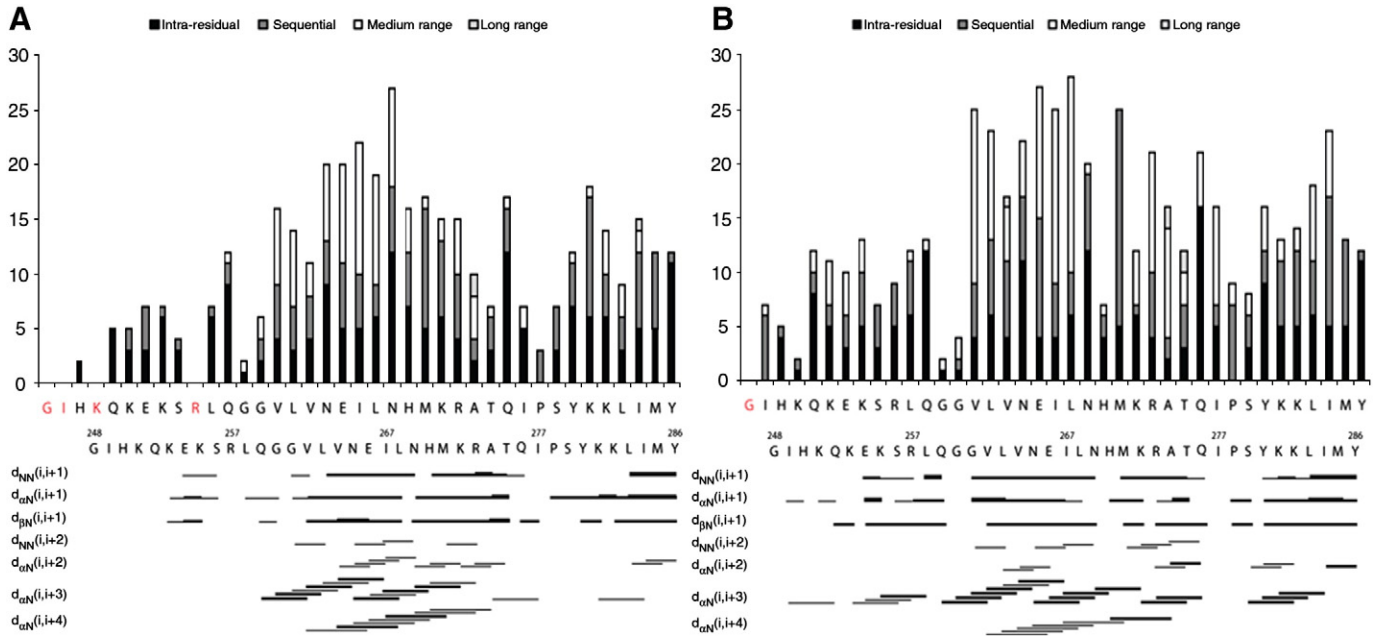

Fig. 7. A summary of NOE connectivities for $PAP_{248-286}$ in 30% TFE (A) and 50% TFE (B). Weak, medium, and strong cross-peaks are represented as lines of increasing thickness.

denatured proteins. The 2D ^{1}H-^{1}H NOESY spectrum of $PAP_{248-286}$ in solution is also consistent with this analysis, as shown by the lack of detectable NOEs and the poor chemical shift dispersion suggestive of an unstructured peptide. Significantly, while medium and long range NOEs are generally not detected for other natively unfolded amyloidogenic peptides [32], chemical shifts and ^{15}N relaxation measurements often give an indication of transient secondary structure [32,35,41].

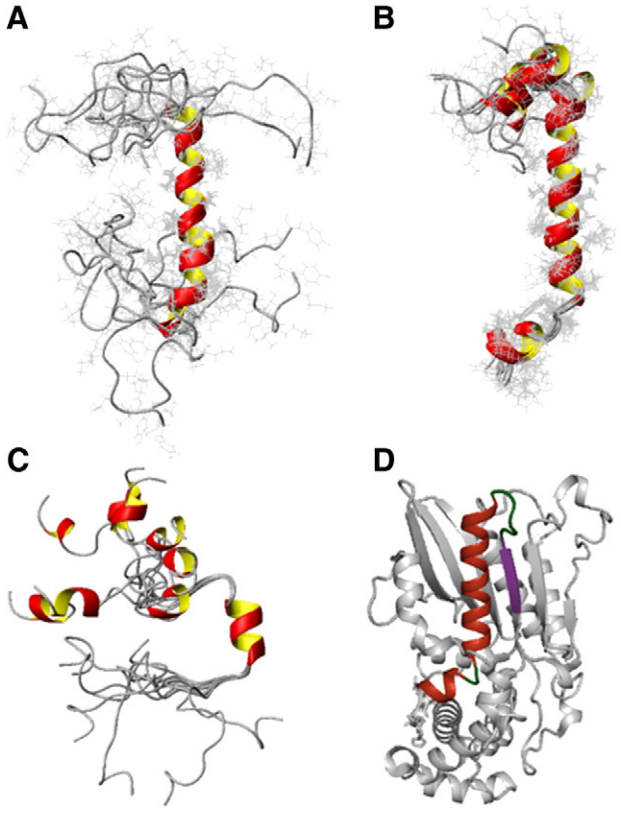

Fig. 8. High-resolution NMR structures of $PAP_{248-286}$ in (A) 30% TFE and (B) 50% TFE, compared to the structure obtained in 200 mM SDS (C) from [12] and the $PAP_{248-286}$ segment in the crystal structure of prostatic acid phosphatase (D) from [66]. In TFE solutions, the protein adopts a largely α-helical structure that differs substantially from the largely disordered structure that exists in SDS micelles or in aqueous solution but is similar to the conformation $PAP_{248-286}$ adopts in the crystal structure of the full-length protein.

The lack of transient secondary structure in $PAP_{248-286}$ in solution may correlate with the difficulty of nucleating formation of the SEVI amyloid form. While $PAP_{248-286}$ will fibrillize readily at high concentrations with orbital shaking [4–7,9,52], it will not fibrillize without agitation of the sample [52]. Agitation is believed to enhance fibrillization by variety of mechanisms, including by breaking up of off-pathway aggregates [53], enhancing the diffusion of large on-pathway intermediates [53], and by increasing the rate of secondary nucleation by breaking existing fibers to provide new nucleation sites [54]. Agitation may also induce secondary structure by increasing the rate at which $PAP_{248-286}$ molecules contact the air/water interface [55]. The need for agitation for $PAP_{248-286}$ to form amyloid fibers may indicate nucleation of the disordered $PAP_{248-286}$ monomer is energetically unfavorable to an unusual degree, consistent with the hypothesis that acquisition of transient secondary structure is a prerequisite for amyloid nucleation.

4.3. The disordered membrane-bound structure of monomeric $PAP_{248-286}$ is unlike that of other amyloidogenic proteins

$PAP_{248-286}$ is also mostly disordered when bound to SDS micelles, with two regions of nascent structure (an α-helix from V262-H270 and a dynamic $\alpha/3_{10}$ helix from S279-L283) which may serve as nuclei for further aggregation as the sequences of these regions are predicted to be highly amyloidogenic. Disordered structures are unusual for membrane binding peptides, most of which adopt α-helical [13–18] or, less commonly, β-hairpin structures [56] initially upon binding. As the membrane-bound structure of $PAP_{248-286}$ is so different from other natively disordered amyloidogenic peptides, a link may exist between the unique structure of membrane-bound $PAP_{248-286}$ and the unique ability of $PAP_{248-286}$ in the amyloid SEVI form to enhance HIV infectivity. Specifically, the conformational flexibility of membrane-bound $PAP_{248-286}$ would enhance the effective radius of capture for incoming viruses, if the conformational

flexibility of the monomer is preserved to some degree in the amyloid form, as has been observed for other amyloid peptides.

4.4. The disordered structure of membrane-bound structure of monomeric $PAP_{248-286}$ is driven by electrostatic factors

The structure of a membrane-bound peptide is determined by a fine balance between hydrophobic and electrostatic factors [57]. Both factors are involved in peptide binding to SDS due to the amphiphilic properties of the SDS molecule; however, the exact degree to which each factor is manifested is dependent on the actual sequence of the peptide. The marked difference between the membrane-bound structure of $PAP_{248-286}$ and those of other amyloidogenic peptides implies the factors stabilizing $PAP_{248-286}$ membrane binding are markedly different from those of other peptides.

Organic solvents such as TFE are useful in dissecting the relative importance of these factors. Trifluoroethanol solutions present a simpler system than SDS micelles and lipid bilayers in which a variety of hydrophobic and electrostatic interactions compete for influence. The mechanism by which trifluoroethanol promotes secondary structure is not completely understood, but is thought to involve either preferential interactions of TFE with the folded state or the displacement of water from the surface of the peptide [58–60]. Both processes have the effect of strengthening internal peptide hydrogen bonds at the expense of solvent-peptide interactions, an effect multiplied by the tendency of fluorinated alcohols to cluster together on the surface of the peptide [59,61]. The low dielectric constant of TFE also plays a role in stabilizing secondary structure by strengthening hydrogen bonds [61,62], although it has been observed that hydrophobic interactions present in the native protein are not significantly disrupted [59]. Studies with many polypeptides suggest the induction of secondary structure by TFE is not indiscriminate but rather reflects the underlying local conformational biases of the peptide [58,63].

Several characteristics of TFE solutions, such as the strengthening of peptide–peptide hydrogen bonds at the expense of peptide–solvent ones and a low dielectric constant, are also reflective of the hydrophobic interior of lipid bilayers [64]. For this reason, TFE has been frequently used as a model of lipid membranes [65,66]. However, there are significant differences between TFE solutions and lipid bilayers that must be considered. One of the most important differences lies in the microstructure of the medium. TFE solutions are uniform in all directions while lipid bilayers have a hydrophobic interior and a polar and charged region near the surface. This difference is important in the binding of amphipathic peptides, as charged residues can interact with the charged surface of the bilayer while, simultaneously, hydrophobic residues can interact with the interior of the bilayer if the distribution of residues is favorable. A comparison between the structures determined in TFE and those determined in bilayers or micelles can therefore establish the effect the intrinsic conformational bias of the primary sequence on the final structure and, by inference, the relative contribution of electrostatic and hydrophobic factors in binding.

$PAP_{248-286}$ is significantly more helical in TFE solutions than in either SDS or aqueous solutions. While only two short regions of helix are detected in SDS micelles (an α-helix from V262-H270 and a dynamic $\alpha/3_{10}$ helix from S279-L283), most of the central region of the peptide is in an α-helix conformation in 30%TFE (Q259-A274) and all of the peptide except for the C-terminal end is in an α-helix conformation in 50% TFE. The high degree of helicity of $PAP_{248-286}$ in TFE solutions suggests that the lack of structure in SDS is not due to an intrinsic conformational bias against helix formation in $PAP_{248-286}$ but rather due to the unique environment of the SDS micelle and, by inference, the unique environment of negatively charged lipid bilayers. As mentioned above, one important difference between TFE and SDS micelles is the absence of an anisotropic environment in TFE solutions that can stabilize the amphipathic nature of a peptide. $PAP_{248-286}$ folds into an amphipathic helix in both 30% and 50% TFE. The structure of $PAP_{248-286}$ in 50% TFE is very similar to structure of the $PAP_{248-286}$ sequence in the crystal structure of the full-length PAP protein, in which a long C-terminal helix (G260-I277) is connected to a shorter N-terminal helix (K251-R257) by a short loop (Fig. 8D) [67], possibly due to the similarities of the dielectric constants of TFE and the interior of the protein. This finding suggests the disordered structure of $PAP_{248-286}$ in SDS is a direct result of the strong binding of $PAP_{248-286}$ to the surface of the micelle where it is stabilized by salt bridges from positively charged residues to the negatively charged headgroup of SDS.

Several lines of evidence argue for an unusual involvement of electrostatic interactions in $PAP_{248-286}$ membrane binding. $PAP_{248-286}$ does not bind to the zwitterionic detergent DPC and does not penetrate into the interior of the SDS micelle as has been seen for other amyloid peptides [12]. The elimination of the membrane permeabilizing activity of $PAP_{248-286}$ by an increase in ionic strength is also in agreement with the superficial attachment of $PAP_{248-286}$ to the membrane surface by electrostatic interactions [68]. The minimal impact on the phase transition of the gel-to-liquid crystalline of liposomes when $PAP_{248-286}$ is incorporated suggests the hydrophobic core of the bilayer is unaffected by $PAP_{248-286}$ binding, arguing against hydrophobic factors having a dominant role [68].

All of these findings are dissimilar to other amyloid peptides, which typically insert fairly deeply into the lipid bilayer when in the form of monomers or small oligomers [69–74]. The importance of electrostatic interactions, as opposed to hydrophobic interactions, in $PAP_{248-286}$ membrane binding is mirrored by their importance in determining the degree to which the SEVI amyloid form enhances infectivity of the HIV virus. A mutant form of SEVI in which the cationic Lys and Arg residues were mutated to Ala failed to enhance HIV infectivity to any degree, despite forming amyloid fibers [5]. Likewise, polyanionic polymers such as heparin compete for binding to SEVI with the membrane of the HIV virus to a degree determined by the amount of sulfonation of the polymer [5]. While electrostatic factors are not the only factors involved in the SEVI-HIV interaction as the cationic polymer surfen eliminates SEVI-HIV binding without disaggregation of the SEVI amyloid fibers [6], they are likely to be dominant in determining the nature of both the structure and binding mode of $PAP_{248-286}$ in the monomeric state. The unusual concentration of positively charged residues in $PAP_{248-286}$ relative to other amyloidogenic peptides may explain the greater dominance of electrostatic interactions over hydrophobic ones [75], and, by inference, $PAP_{248-286}$ unusual potency in enhancing viral infectivity.

Supplementary materials related to this article can be found online at doi:10.1016/j.bbamem.2011.01.010.

Acknowledgments

This study was supported by research funds from NIH (DK078885 to A. R.). We thank the 900 MHz NMR facility at the Michigan State University.

References

[1] A.S. Chuck, M.F. Clarke, B.O. Palsson, Retroviral infection is limited by Brownian motion, Hum. Gene Ther. 7 (1996) 1527–1534.
[2] A.S. Perelson, A.U. Neumann, M. Markowitz, J.M. Leonard, D.D. Ho, HIV-1 dynamics in vivo: virion clearance rate, infected cell life-span, and viral generation time, Science 271 (1996) 1582–1586.
[3] J.A. Thomas, D.E. Ott, R.J. Gorelick, Efficiency of human immunodeficiency virus type 1 postentry infection processes: Evidence against disproportionate numbers of defective virions, J. Virol. 81 (2007) 4367–4370.
[4] J. Munch, E. Rucker, L. Standker, K. Adermann, C. Goffinet, M. Schindler, S. Wildum, R. Chinnadurai, D. Rajan, A. Specht, G. Gimenez-Gallego, P.C. Sanchez, D.M. Fowler, A. Koulov, J.W. Kelly, W. Mothes, J.C. Grivel, L. Margolis, O.T. Keppler, W.G. Forssmann, F. Kirchhoff, Semen-derived amyloid fibrils drastically enhance HIV infection, Cell 131 (2007) 1059–1071.

[5] N.R. Roan, J. Munch, N. Arhel, W. Mothes, J. Neidleman, A. Kobayashi, K. Smith-McCune, F. Kirchhoff, W.C. Greene, The cationic properties of SEVI underlie its ability to enhance human immunodeficiency virus infection, J. Virol. 83 (2009) 73–80.
[6] N.R. Roan, S. Sowinski, J. Munch, F. Kirchhoff, W.C. Greene, Aminoquinoline surfen inhibits the action of SEVI (semen-derived enhancer of viral infection), J. Biol. Chem. 285 (2010) 1861–1869.
[7] S.H. Hong, E.A. Klein, J. Das Gupta, K. Hanke, C.J. Weight, C. Nguyen, C. Gaughan, K.A. Kim, N. Bannert, F. Kirchhoff, J. Munch, R.H. Silverman, Fibrils of prostatic acid phosphatase fragments boost infections with XMRV (xenotropic murine leukemia virus-related virus), a human retrovirus associated with prostate cancer, J. Virol. 83 (2009) 6995–7003.
[8] M. Wurm, A. Schambach, D. Lindemann, H. Hanenberg, L. Standker, W.G. Forssmann, R. Blasczyk, P.A. Horn, The influence of semen-derived enhancer of virus infection on the efficiency of retroviral gene transfer, J. Gene Med. 12 (2010) 137–146.
[9] I. Hauber, H. Hohenberg, B. Holstermann, W. Hunstein, J. Hauber, The main green tea polyphenol epigallocatechin-3-gallate counteracts semen-mediated enhancement of HIV infection, Proc. Natl Acad. Sci. USA 106 (2009) 9033–9038.
[10] K.A. Kim, M. Yolamanova, O. Zirafi, N.R. Roan, L. Standker, W.G. Forssmann, A. Burgener, N. Dejucq-Rainsford, B.H. Hahn, G.M. Shaw, W.C. Greene, F. Kirchhoff, J. Muench, Semen-mediated enhancement of HIV infection is donor-dependent and correlates with the levels of SEVI, Retrovirology 7 (2010) 55–67.
[11] W.M. Wojtowicz, M. Farzan, J.L. Joyal, K. Carter, G.J. Babcock, D.I. Israel, J. Sodroski, T. Mirzabekov, Stimulation of enveloped virus infection by beta-amyloid fibrils, J. Biol. Chem. 277 (2002) 35019–35024.
[12] R.P.R. Nanga, J.R. Brender, S. Vivekanandan, N. Popovych, A. Ramamoorthy, NMR structure in a membrane environment reveals putative amyloidogenic regions of the SEVI precursor peptide PAP(248–286), J. Am. Chem. Soc. 131 (2009) 17972–17979.
[13] M. Coles, W. Bicknell, A.A. Watson, D.P. Fairlie, D.J. Craik, Solution structure of amyloid beta-peptide(1–40) in a water-micelle environment. Is the membrane-spanning domain where we think it is? Biochemistry 37 (1998) 11064–11077.
[14] A. Motta, G. Andreotti, P. Amodeo, G. Strazzullo, M.A.C. Morelli, Solution structure of human calcitonin in membrane-mimetic environment: the role of the amphipathic helix, Proteins 32 (1998) 314–323.
[15] A. Olofsson, T. Borowik, G. Grobner, A.E. Sauer-Eriksson, Negatively charged phospholipid membranes induce amyloid formation of medin via an alpha-helical intermediate, J. Mol. Biol. 374 (2007) 186–194.
[16] M. Bisaglia, A. Trolio, M. Bellanda, E. Bergantino, L. Bubacco, S. Mammi, Structure and topology of the non-amyloid-beta component fragment of human alpha-synuclein bound to micelles: Implications for the aggregation process, Protein Sci. 15 (2006) 1408–1416.
[17] T.S. Ulmer, A. Bax, N.B. Cole, R.L. Nussbaum, Structure and dynamics of micelle-bound human alpha-synuclein, J. Biol. Chem. 280 (2005) 9595–9603.
[18] S.M. Patil, S.H. Xu, S.R. Sheftic, A.T. Alexandrescu, Dynamic alpha-helix structure of micelle-bound human amylin, J. Biol. Chem. 284 (2009) 11982–11991.
[19] T.R. Dafforn, C.J. Smith, Natively unfolded domains in endocytosis: hooks, lines and linkers, EMBO Rep. 5 (2004) 1046–1052.
[20] B.A. Shoemaker, J.J. Portman, P.G. Wolynes, Speeding molecular recognition by using the folding funnel: the fly-casting mechanism, Proc. Natl Acad. Sci. USA 97 (2000) 8868–8873.
[21] P. Tompa, Structural disorder in amyloid fibrils: its implication in dynamic interactions of proteins, FEBS J. 276 (2009) 5406–5415.
[22] D. Hall, N. Hirota, C.M. Dobson, A toy model for predicting the rate of amyloid formation from unfolded protein, J. Mol. Biol. 351 (2005) 195–205.
[23] J.E. Tanner, Use of stimulated echo in NMR-diffusion studies, J. Chem. Phys. 52 (1970) 2523–2526.
[24] R. Mills, Self-diffusion in normal and heavy-water in range 1–45 degrees, J. Phys. Chem. 77 (1973) 685–688.
[25] M. Piotto, V. Saudek, V. Sklenar, Gradient-tailored excitation for single-quantum NMR-spectroscopy of aqueous-solutions, J. Biomol. NMR 2 (1992) 661–665.
[26] K. Wuthrich (Ed.), NMR of proteins and nucleic acids, John Wiley and Sons, New York, 1986.
[27] T.D. Goddard, D.G. Kneller, SPARKY 3, University of California, San Francisco, 1999.
[28] F. Delaglio, S. Grzesiek, G.W. Vuister, G. Zhu, J. Pfeifer, A. Bax, NMRPipe: A multidimensional spectral processing system based on UNIX pipes, J. Biomol. NMR 6 (1995) 277–293.
[29] G. Cornilescu, F. Delaglio, A. Bax, Protein backbone angle restraints from searching a database for chemical shift and sequence homology, J. Biomol. NMR 13 (1999) 289–302.
[30] T. Herrmann, P. Guntert, K. Wuthrich, Protein NMR structure determination with automated NOE assignment using the new software CANDID and the torsion angle dynamics algorithm DYANA, J. Mol. Biol. 319 (2002) 209–227.
[31] R. Koradi, M. Billeter, K. Wuthrich, MOMOL: a program for display and analysis of macromolecular structures, J. Mol. Graph. Model. 14 (1996) 51–55.
[32] I.T. Yonemoto, G.J. Kroon, H.J. Dyson, W.E. Balch, J.W. Kelly, Amylin proprotein processing generates progressively more amyloidogenic peptides that initially sample the helical state, Biochemistry 47 (2008) 9900–9910.
[33] H.Y. Kim, H. Heise, C.O. Fernandez, M. Baldus, M. Zweckstetter, Correlation of amyloid fibril beta-structure with the unfolded state of alpha-synuclein, Chembiochem 8 (2007) 1671–1674.
[34] D. Eliezer, P. Barre, M. Kobaslija, D. Chan, X.H. Li, L. Heend, Residual structure in the repeat domain of tau: echoes of microtubule binding and paired helical filament formation, Biochemistry 44 (2005) 1026–1036.
[35] J. Danielsson, J. Jarvet, P. Damberg, A. Graslund, The Alzheimer beta-peptide shows temperature-dependent transitions between left-handed 3(1)-helix, beta-strand and random coil secondary structures, FEBS J. 272 (2005) 3938–3949.
[36] K.P. Wu, S. Kim, D.A. Fela, J. Baum, Characterization of conformational and dynamic properties of natively unfolded human and mouse alpha-synuclein ensembles by NMR: Implication for aggregation, J. Mol. Biol. 378 (2008) 1104–1115.
[37] J.A. Williamson, A.D. Miranker, Direct detection of transient alpha-helical states in islet amyloid polypeptide, Protein Sci. 16 (2007) 110–117.
[38] Y.H. Sung, D. Eliezer, Residual structure, backbone dynamics, and interactions within the synuclein family, J. Mol. Biol. 372 (2007) 689–707.
[39] L.M. Hou, H.Y. Shao, Y.B. Zhang, H. Li, N.K. Menon, E.B. Neuhaus, J.M. Brewer, I.J.L. Byeon, D.G. Ray, M.P. Vitek, T. Iwashita, R.A. Makula, A.B. Przybyla, M.G. Zagorski, Solution NMR studies of the Aβ(1–40) and Aβ(1–42) peptides establish that the met35 oxidation state affects the mechanism of amyloid formation, J. Am. Chem. Soc. 126 (2004) 1992–2005.
[40] R. Bussell, D. Eliezer, Residual structure and dynamics in Parkinson's disease-associated mutants of alpha-synuclein, J. Biol. Chem. 276 (2001) 45996–46003.
[41] J. Danielsson, A. Andersson, J. Jarvet, A. Graslund, N-15 relaxation study of the amyloid beta-peptide: structural propensities and persistence length, Magn. Reson. Chem. 44 (2006) S114–S121.
[42] R. Soong, J.R. Brender, P.M. Macdonald, A. Ramamoorthy, Association of highly compact type ii diabetes related islet amyloid polypeptide intermediate species at physiological temperature revealed by diffusion NMR spectroscopy, J. Am. Chem. Soc. 131 (2009) 7079–7085.
[43] S. Narayanan, B. Reif, Characterization of chemical exchange between soluble and aggregated states of beta-amyloid by solution-state NMR upon variation of salt conditions, Biochemistry 44 (2005) 1444–1452.
[44] D.K. Wilkins, S.B. Grimshaw, V. Receveur, C.M. Dobson, J.A. Jones, L.J. Smith, Hydrodynamic radii of native and denatured proteins measured by pulse field gradient NMR techniques, Biochemistry 38 (1999) 16424–16431.
[45] J.D. Knight, J.A. Hebda, A.D. Miranker, Conserved and cooperative assembly of membrane-bound alpha-helical states of islet amyloid polypeptide, Biochemistry 45 (2006) 9496–9508.
[46] R.S. Harrison, P.C. Sharpe, Y. Singh, D.P. Fairlie, Amyloid peptides and proteins in review, Rev. Physiol. Biochem. P 159 (2007) 1–77.
[47] V.N. Uversky, A.L. Fink, Conformational constraints for amyloid fibrillation: the importance of being unfolded, Biochim. Biophys. Acta 1698 (2004) 131–153.
[48] A. Abedini, D.P. Raleigh, A critical assessment of the role of helical intermediates in amyloid formation by natively unfolded proteins and polypeptides, Protein Eng. Des. Sel. 22 (2009) 453–459.
[49] V.N. Uversky, J. Li, A.L. Fink, Evidence for a partially folded intermediate in alpha-synuclein fibril formation, J. Biol. Chem. 276 (2001) 10737–10744.
[50] M.D. Kirkitadze, M.M. Condron, D.B. Teplow, Identification and characterization of key kinetic intermediates in amyloid beta-protein fibrillogenesis, J. Mol. Biol. 312 (2001) 1103–1119.
[51] R. Bystrom, C. Aisenbrey, T. Borowik, M. Bokvist, F. Lindstrom, M.A. Sani, A. Olofsson, G. Grobner, Disordered proteins: Biological membranes as two-dimensional aggregation matrices, Cell Biochem. Biophys. 52 (2008) 175–189.
[52] Z.Q. Ye, K.C. French, L.A. Popova, I.K. Lednev, M.M. Lopez, G.I. Makhatadze, Mechanism of fibril formation by a 39-residue peptide (PAPf39) from human prostatic acidic phosphatase, Biochemistry 48 (2009) 11582–11591.
[53] T.R. Serio, A.G. Cashikar, A.S. Kowal, G.J. Sawicki, J.J. Moslehi, L. Serpell, M.F. Arnsdorf, S.L. Lindquist, Nucleated conformational conversion and the replication of conformational information by a prion determinant, Science 289 (2000) 1317–1321.
[54] L. Giehm, D.E. Otzen, Strategies to increase the reproducibility of protein fibrillization in plate reader assays, Anal. Biochem. 400 (2010) 270–281.
[55] A. Morinaga, K. Hasegawa, R. Nomura, T. Ookoshi, D. Ozawa, Y. Goto, M. Yamada, H. Naiki, Critical role of interfaces and agitation on the nucleation of A beta amyloid fibrils at low concentrations of A beta monomers, BBA Prot. Proteom. 1804 (2010) 986–995.
[56] L.P. Yu, R. Edalji, J.E. Harlan, T.F. Holzman, A.P. Lopez, B. Labkovsky, H. Hillen, S. Barghorn, U. Ebert, P.L. Richardson, L. Miesbauer, L. Solomon, D. Bartley, K. Walter, R.W. Johnson, P.J. Hajduk, E.T. Olejniczak, Structural characterization of a soluble amyloid beta-peptide oligomer, Biochemistry 48 (2009) 1870–1877.
[57] R. Montserret, M.J. McLeish, A. Bockmann, C. Geourjon, F. Penin, Involvement of electrostatic interactions in the mechanism of peptide folding induced by sodium dodecyl sulfate binding, Biochemistry 39 (2000) 8362–8373.
[58] M. Buck, Trifluoroethanol and colleagues: cosolvents come of age. Recent studies with peptides and proteins, Q. Rev. Biophys. 31 (1998) 297–355.
[59] D. Roccatano, G. Colombo, M. Fioroni, A.E. Mark, Mechanism by which 2, 2, 2-trifluoroethanol/water mixtures stabilize secondary-structure formation in peptides: A molecular dynamics study, Proc. Natl Acad. Sci. USA 99 (2002) 12179–12184.
[60] R. Walgers, T.C. Lee, A. Cammers-Goodwin, An indirect chaotropic mechanism for the stabilization of helix conformation of peptides in aqueous trifluoroethanol and hexafluoro-2-propanol, J. Am. Chem. Soc. 120 (1998) 5073–5079.
[61] D.P. Hong, M. Hoshino, R. Kuboi, Y. Goto, Clustering of fluorine-substituted alcohols as a factor responsible for their marked effects on proteins and peptides, J. Am. Chem. Soc. 121 (1999) 8427–8433.
[62] N. Javid, K. Vogtt, C. Krywka, M. Tolan, R. Winter, Protein-protein interactions in complex cosolvent solutions, Chemphyschem 8 (2007) 679–689.
[63] P.Z. Luo, R.L. Baldwin, Mechanism of helix induction by trifluoroethanol: A framework for extrapolating the helix-forming properties of peptides from

trifluoroethanol/water mixtures back to water, Biochemistry 36 (1997) 8413–8421.
[64] V.E. Bychkova, A.E. Dujsekina, S.I. Klenin, E.I. Tiktopulo, V.N. Uversky, O.B. Ptitsyn, Molten globule-like state of cytochrome c under conditions simulating those near the membrane surface, Biochemistry 35 (1996) 6058–6063.
[65] O. Crescenzi, S. Tomaselli, R. Guerrini, S. Salvadori, A.M. D'Ursi, P.A. Temussi, D. Picone, Solution structure of the Alzheimer amyloid beta-peptide (1–42) in an apolar microenvironment - Similarity with a virus fusion domain, Eur. J. Biochem. 269 (2002) 5642–5648.
[66] L.A. Munishkina, C. Phelan, V.N. Uversky, A.L. Fink, Conformational behavior and aggregation of alpha-synuclein in organic solvents: Modeling the effects of membranes, Biochemistry 42 (2003) 2720–2730.
[67] C.G. Jakob, K. Lewinski, R. Kuciel, W. Ostrowski, L. Lebioda, Crystal structure of human prostatic acid phosphatase, Prostate 42 (2000) 211–218.
[68] J.R. Brender, K. Hartman, L.M. Gottler, M.E. Cavitt, D.W. Youngstrom, A. Ramamoorthy, Helical conformation of the SEVI precursor peptide PAP(248–286), a dramatic enhancer of hiv infectivity, promotes lipid aggregation and fusion, Biophys. J. 97 (2009) 2474–2483.
[69] J.R. Brender, K. Hartman, K.R. Reid, R.T. Kennedy, A. Ramamoorthy, A single mutation in the nonamyloidogenic region of islet amyloid polypeptide greatly reduces toxicity, Biochemistry 47 (2008) 12680–12688.
[70] R.P.R. Nanga, J.R. Brender, J.D. Xu, G. Veglia, A. Ramamoorthy, Structures of rat and human islet amyloid polypeptide IAPP(1–19) in micelles by NMR spectroscopy, Biochemistry 47 (2008) 12689–12697.
[71] M.F.M. Engel, H. Yigittop, R.C. Elgersma, D.T.S. Rijkers, R.M.J. Liskamp, B. de Kruijff, J.W.M. Hoppener, J.A. Killian, Islet amyloid polypelptide inserts into phospholipid monolayers as monomer, J. Mol. Biol. 356 (2006) 783–789.
[72] M.F.M. Sciacca, M. Pappalardo, D. Milardi, D.M. Grasso, C. La Rosa, Calcium-activated membrane interaction of the islet amyloid polypeptide: Implications in the pathogenesis of type II diabetes mellitus, Arch. Biochem. Biophys. 477 (2008) 291–298.
[73] R.H. Ashley, T.A. Harroun, T. Hauss, K.C. Breen, J.P. Bradshaw, Autoinsertion of soluble oligomers of Alzheimer's Aβ(1–42) peptide into cholesterol-containing membranes is accompanied by relocation of the sterol towards the bilayer surface, BMC Struct. Biol. 6 (2006) 21–31.
[74] J. Varkey, J.M. Isas, N. Mizuno, M.B. Jensen, V.K. Bhatia, C.C. Jao, J. Petrlova, J.C. Voss, D.G. Stamou, A.C. Steven, R. Langen, Membrane curvature induction and tubulation are common features of synucleins and apolipoproteins, J. Biol. Chem. 285 (2010) 32486–32493.
[75] K.F. DuBay, A.P. Pawar, F. Chiti, J. Zurdo, C.M. Dobson, M. Vendruscolo, Prediction of the absolute aggregation rates of amyloidogenic polypeptide chains, J. Mol. Biol. 341 (2004) 1317–1326.